韓國鑛物學會誌 第 11 卷 第 1 號 (1998)
J. Miner. Soc. Korea, 11, 45-67 (1998)

FORTRAN Program "PHYLS" for the Geometrical Prediction of the Structures of 1M and $2M_1$ 2:1 Phyllosilicates Having Space Groups C2/m, C2, and C2/c

공간군 C2/m, C2, 및 C2/c를 갖는 1M 및 $2M_1$ 2:1 층상 규산염 광물 구조의 기하학적 예측을 위한 포트란 프로그램 "PHYLS"

Jae-Young Yu (유재영)* · M. Slaughter**

*Department of Geology, Kangwon National University, Chuncheon, Kangwon-Do 200-701, Korea
(강원대학교 지질학과)
**Department of Chemistry and Geochemistry, Colorado School of Mines,
Golden, Colorado 80401, U.S.A.

ABSTRACT : FORTRAN program PHYLS was developed to model the structures of 2:1 1M and $2M_1$ phyllosilicates on the basis of geometrical analyses. Input to PHYLS requires the chemical composition and d(001) spacing of the mineral. The output from PHYLS consists of the coordinates of the crystallographically independent sites in the unit cell, and such structural parameters as the cell dimensions, interaxial angle, cell volume, interatomic distances, and deformation angles of the polyhedra. PHYLS can generate these structural details according to the user's choice of space group and cation configuration. User can choose one of such space groups as C2/m, C2, and C2/c and such cation configurations as random and ordered tetrahedral/octahedral cation configurations. PHYLS simulated the structures of dioctahedral and trioctahedral phyllosilicates having random tetrahedral cation configuration fairly close to the reported experimentally determined structures. In contrast, the simulated structures for ordered tetrahedral cation configurations showed greater deviation from the experimentally determined structures than those for random configurations. However, if the cations were partially ordered and the sizes of the tetrahedra became similar, the simulated structures showed little deviations from the experimental ones, which suggests that appropriate application of PHYLS may be helpful in various investigations on the relationships between structures and physicochemical properties of the phyllosilicates.

요약 : 기하학적 분석을 바탕으로 1M 및 $2M_1$ 2:1 층상 규산염 광물의 구조를 모델링 하기 위한 포트란 프로그램 PHYLS가 개발되었다. PHYLS를 수행하기 위한 입력자료는 광물의 화학 조성과 d(001) 격자 거리이며, 이로부터의 출력은 단위포 내 결정학적 독립 구조 자리의 위치, 그리고 단위포의 크기 및 부피, 축각, 원자간 거리, 다면체의 변형 각도등을 포함하는 구조적 요소들이다. PHYLS는 이와 같은 자세한 구조 정보를 사용자가 선택하는 공간군 및 양이온 분포 등에 따라서 계산하여 준다. 사용자가 선택할 수 있는 공간군은 C2/m, C2, 및 C2/c이며, 또한 사용자가 선택할 수 있는 양이온의 분포는 사면체 및 팔면체 양이온의 무작위 분포와 규칙적 분포이다. 무작위 양이온 분포를 갖는 이팔면체 및 삼팔면체 층상 규산염 광물들에 대해 PHYLS가 예측한 구조는 실제 보고된 구조와 상당히 일치하는 반면, 규칙적인 양이온 분포를 갖는 층상 규산염 광물에 대해 예측된 구조는 실험적으로 보고된 것과 어느 정도 차이를 보이고 있다. 그러나, 양이온들이 부분적인 규칙적 배열을 함에 따라 사면체 간의 크기 차이가 적어지면, PHYLS에 의해 예측

된 구조와 실험적으로 보고된 구조는 거의 일치하게 된다. 이는 층상 규산염 광물의 구조와 물리화학적 성질의 관계에 대한 다양한 연구에 PHYLS를 적절히 사용한다면 크게 도움이 될 수 있음을 지시한다 하겠다.

INTRODUCTION

Many investigators have attempted to find a universal model capable of predicting the structure of the phyllosilicate having any chemical composition and structural symmetry, because the accurate experimental determination of its structure has been often difficult or sometimes impossible due to its poor crystallinity and/or very fine crystal size. Out of a few, geometrical approach is the most frequently used to construct the structural model. Franzini and Schiaffino (1963), Donnay et al. (1964), Tepkin et al. (1969), and Appelo (1978) analyzed the geometries of the polyhedra to simulate the structures of phyllosilcates for 1M trioctahedral micas and Appelo (1978) for $2M_1$ dioctahedral micas. They successfully predicted the structural details of the minerals in agreement with the experimentally determined ones, but their models require the cell parameters such as b, c and β, which are difficult to obtain, and insufficiently sensitive to the chemistries of the minerals. Recently, Yu (1990) and Smoliar-Zviagina (1993) constructed geometrical structural models for 1M trioctahedral phyllosilicates and $2M_1$, 3T, and 1M dioctahedral micas, respectively. Both models of Yu (1990) and Smoliar-Zviagina (1993) can predict the structures without any difficult-to-obtain structural parameters, but their models again have limitations in structural variability and chemical compositional ranges for application, respectively. The simulation of phyllosilicate structures had been also attempted with energy minimization approach. Collins and Catlow (1992) simulated the mica structures, using computational energy and free-energy minimization techniques, but such energy minimization method can not predict the structure as accurate as the geometrical method yet.

The purpose of this study is to construct an universal model which can predict the structural details of 2:1 phyllosilicates of any chemical composition and encode the simulation procedures of the model in FORTRAN for quick and easy application. "PHYLS" is the FORTRAN program for the purpose of such structural simulation. Input to PHYLS requires only the chemical composition and d(001) spacing of the mineral. The d(001) spacing can be easily determined by powder x-ray diffraction analyses.

The structural model of this study starts from the following assumptions now well recognized to be possibly true among mineralogists:

1. Because of repulsion between the octahedral cations, the octahedral layer is stretched and flattened (octahedral deformation), but maintains regular hexagonal configuration on (001) (Bailey, 1984).

2. r_o remains constant during the octahedral deformation (Donnay et al., 1964).

3. The orthohexagonal relation $a=b\tan 30°$ is rigorously obeyed (Sadanaga and Takeuchi, 1961).

4. The misfit in size between the tetrahedral and octahedral layer is relieved by tetrahedral rotation and tetrahedral tilting adjusts the positions of the apical oxygens to be shared by the tetrahedral and octahedral layer (Bailey, 1984).

GEOMETRICAL STRUCTURE SIMULATION

Fig. 1 depicts the outlines of the simulation processes of PHYLS. The following are the detailed descriptions of the simulation processes.

Data Input

Table 1 summarizes the necessary input data for PHYLS. Of all input data, the chemical composition of the mineral is the most important one, because it determines interatomic distances, the b-dimension, and thus, all the details of the structural parameters including the deformation of polyhedra. The chemical composition excludes some trace, but occasionally found components, such as Li, Ti, Mn, Zn, Ba, and NH_4^+. If one chooses an ordered tetrahedral cation configuration, the mole fraction of each cation in each tetrahedral cation site must be provided. The optional space groups of the mineral are C2/m and C2/c for a random tetrahedral cation configuration and C2 and C2/c for ordered tetrahedral cation configurations. The ordered octahedral cation configuration can be chosen only for trioctahedral minerals. If one chooses an ordered octahedral cation configuration, the program will automatically distribute cations over the octahedral site in such a way that Al first occupies the site I as much as possible, and the remaining cations evenly distribute over the sites I and II.

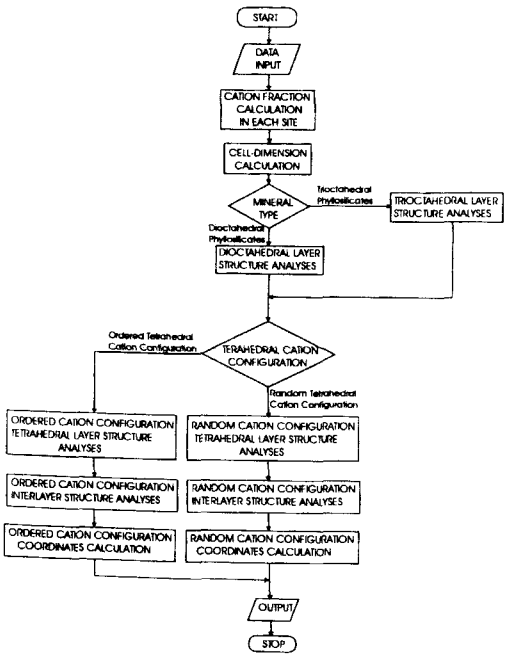

Fig. 1. Computational scheme of program PHYLS.

Cell Dimension Calculation

PHYLS calculates the b-dimension from the chemical compositions with regression equations. A number of regression equations have been reported (Faust, 1957; Radoslovich, 1962; Veitch and Radoslovich, 1963; Frey et al., 1983; Guidotti, 1984; Drits and Zviagina, 1992). PHYLS uses the equation of Veitch and Radoslovitch (1963) for dioctahedral micas and that of Radoslovitch (1962) for smectites and trioctahedral micas, but one may use other equations to improve specific simulations. The equation of Veitch and Radoslovich (1963) for dioctahedral micas is given by

$$b = 9.114 + 0.2849u_{11} + 0.8106u_1 - 0.4207u_{21} - 0.5003u_{22} - 0.4402u_{23}, \quad (1)$$

where

$u_{11} = 1.33n_K + 0.95n_{Na} + 0.99n_{Ca}$,

$u_1 = 0.75n_{Fe^{2+}} + 0.65n_{Mg} + 0.5n_{[6]Al} + 0.65n_{Mg*}$

(n_{Mg*} is the number of trioctahedral Mg),

$u_{21} = n_k + n_{Na} + n_{Ca}$,

$u_{22} = n_{Fe^{2+}} + n_{Mg}$, and

Table 1. Input data for PHYLS.

Codes	Descriptions	Options
NAME	comments on the mineral	
MIN	type of the phyllosilicates	1=dioctahedral mica 2=trioctahedral mica 3=dioctahedral smectite 4=trioctahedral smectite
JS	tetrahedral cation configuration	1=random 2=ordered
JOS	octahedral cation configuration	only for MIN=2 or 4 1=random 2=ordered
IS	space group	if JS=1, 1=C2/m, 2=C2/c if JS=2, 1=C2, 2=C2/c
FRTN4(i)	number of the tetrahedral cations in the structural chemical formula	i=1 (Si), 2 (Al), 3(Fe^{3+})
FRTN6(j)	number of the octahedral cations in the structural chemical formula	j=1 (Al), 2 (Fe^{3+}), 3 (Fe^{2+}), 4 (Mg)
FRTNI(k)	number of the interlayer cations in the structural chemical formula	k=1 (K), 2 (Na), 3 (Ca)
FRTN4O(m, i)	fractions of the tetrahedral cations in site I (m=1) and II (m=2).	only for JS=2
CP	d(001) for 1M or d(002) for $2M_1$ phyllosilicates	

$$u_{23} = n_{[6]Al} + n_{[6]Fe^{3+}} + n_{Mg^{*}}.$$

The equations of Radoslovich (1962) for trioctahedral micas and smectites are respectively

$$b = 8.925 + 0.099n_K - 0.069n_{Ca} + 0.062n_{Mg} + 0.116n_{Fe^{2+}} + 0.098n_{[6]Fe^{3+}} \text{ and} \quad (2)$$

$$b = 8.944 + 0.096n_{Mg} + 0.096n_{[6]Fe^{3+}} + 0.037n_{[4]Al}. \quad (3)$$

After the calculation of the b-dimension, the a-dimension is calculated with the following orthohexagonal relation;

$$a = b\tan(30°). \quad (4)$$

The c-dimension is calculated from the given d(001) and geometrically calculated β, as elaborated in the interlayer structure analysis section:

$$c = \frac{d(001)}{\sin(\beta)}. \quad (5)$$

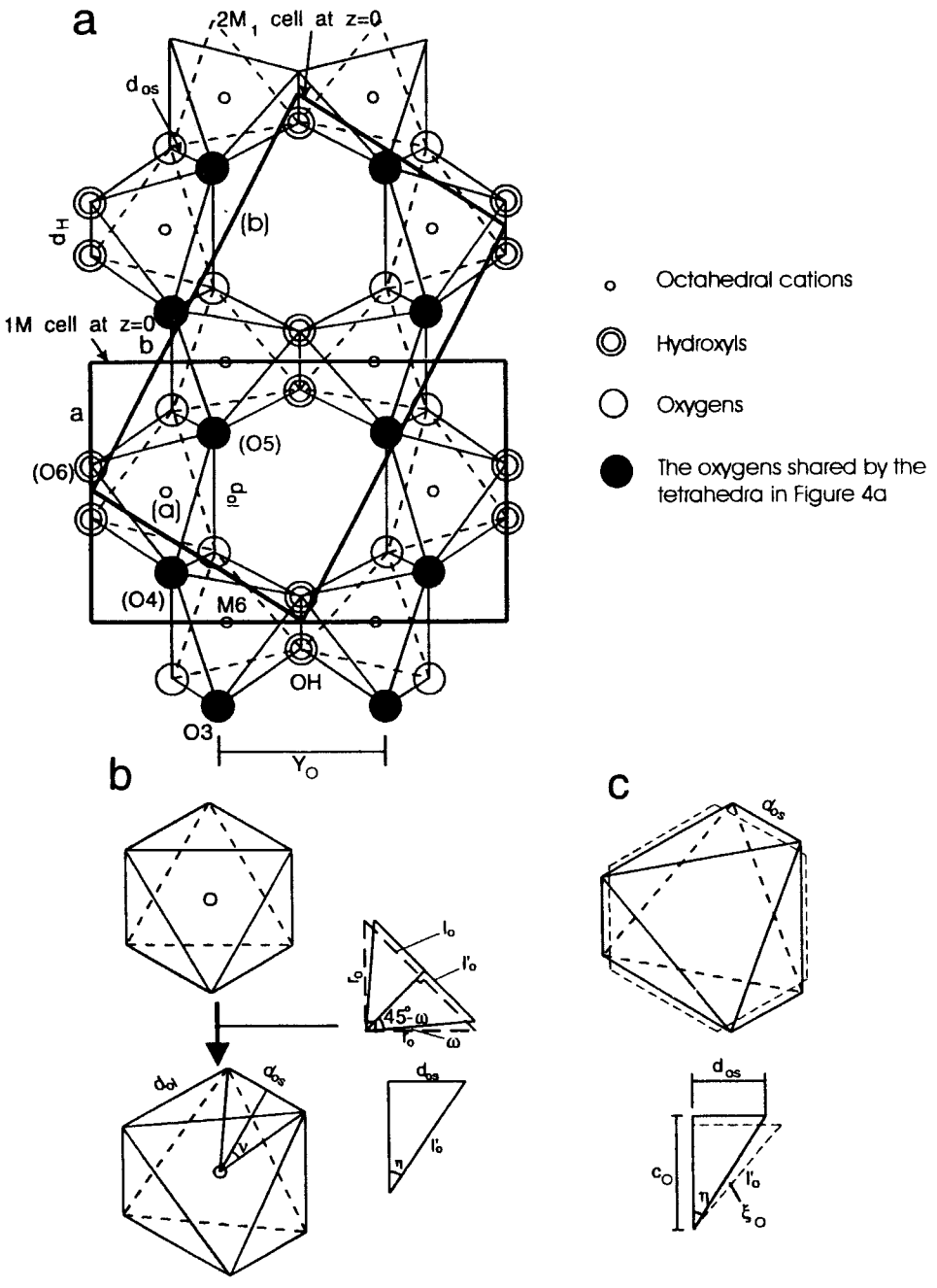

Fig. 2. Geometry of the atomic arrangement in the dioctahedral layer. a: Overall view of the atomic arrangement projected on (001). b: Octahedral flattening by an angle ω. c: Increase in the vertical angle of the octahedral edge by an angle ξ. The octahedra of broken and solid lines represent the octahedra before and after the vertical angle increase, respectively.

Dioctahedral Layer Structure Analyses

Fig. 2 shows the geometry of the atomic distribution in the dioctahedral layer. The geometry of the unit cell (Fig. 2a) gives

$$b=\sqrt{3}\,(d_{os}+2d_{ol}). \tag{6}$$

In equation (6), d_{os} and d_{ol} are respectively given by

$$d_{os}=\frac{2r_o\sin(45^\circ-\omega)}{\sqrt{3}}, \text{ and} \tag{7}$$

$$d_{ol}=2\sqrt{\left(\frac{d_{os}}{2}\right)^2+(r_o\cos(45^\circ-\omega))^2}\,\sin(60^\circ-\nu), \tag{8}$$

where

$$\nu=a\cos\left(\frac{r_o\cos(45^\circ-\omega)}{\sqrt{(d_{os}/2)^2+(r_o\cos(45^\circ-\omega))^2}}\right) \text{ (Fig. 2b).}$$

If the octahedral cations randomly distribute, r_o in equations (7) and (8) may be expressed as

$$r_o=\sum_i f_{o,i}r_{o,i} \tag{9}$$

Table 2 lists not only $r_{o,i}$ but also $r_{t,j}$ used in the calculation. Most of the bond lengths in Table 2 are adapted from the values of Shannon (1976), but some of them are modified according to the observed interatomic distances of micas by many investigators. Solutions of equations (6) to (9), d_{os}, d_{ol}, and w are obtained by iterative calculation. Then, the shorter octahedral edge length becomes

$$l_o'=2r_o\sin(45^\circ-\omega). \tag{10}$$

Simple flattening by ω, as calculated above produces a little thinner simulated octahedral layer than the observed ones. Thus, the simulated octahedra require additional deformation,

Table 2. Interatomic distances used in the structure prediction by PHYLS.

Structural Unit	Atomic Pair	Interatomic Distance (Å)
Tetrahedral layer	Si-O	1.610
($r_{t,j}$)	Al-O	1.745
	Fe^{3+}-O	1.840
Otahedral layer	Al-O	1.920
($r_{o,i}$)	Fe^{3+}-O	2.000
	Fe^{2+}-O	2.130
	Mg-O	2.060

which increases its thickness, while r_o remains constant. This can be done by increase the vertical angle of the octahedral edge (Fig. 2c). Empirical fitting of the calculated z-coordinates of the oxygens to the reported ones indicates that the amount of increase in the vertical angle is proportional to the flattening angle in such a way that

$$\xi_O=\frac{\omega}{0.87}, \text{ and} \tag{11}$$

$$\xi_H=\frac{\omega}{3.7} \tag{12}$$

Due to the increase in the vertical angle of the octahedral edge, the octahedral edge lengths projected on (001) must be recalculated as follows:

$$d_{os}=l_o'\sin(\eta-\xi_O), \tag{13}$$

$$d_H=l_o'\sin(\eta-\xi_H), \text{ and} \tag{14}$$

$$d_{ol}=2\sin(60^\circ-\nu)\sqrt{\left(\frac{d_{os}}{2}\right)^2+(r_o\cos(45^\circ-\omega))^2}, \tag{15}$$

where

$$\eta=a\sin\left(\frac{1}{\sqrt{3}}\right), \text{ and}$$

$$\nu=a\cos\left(\frac{r_o\cos(45^\circ-\omega)}{\sqrt{(d_{os}/2)^2+(r_o\cos(45^\circ-\omega))^2}}\right).$$

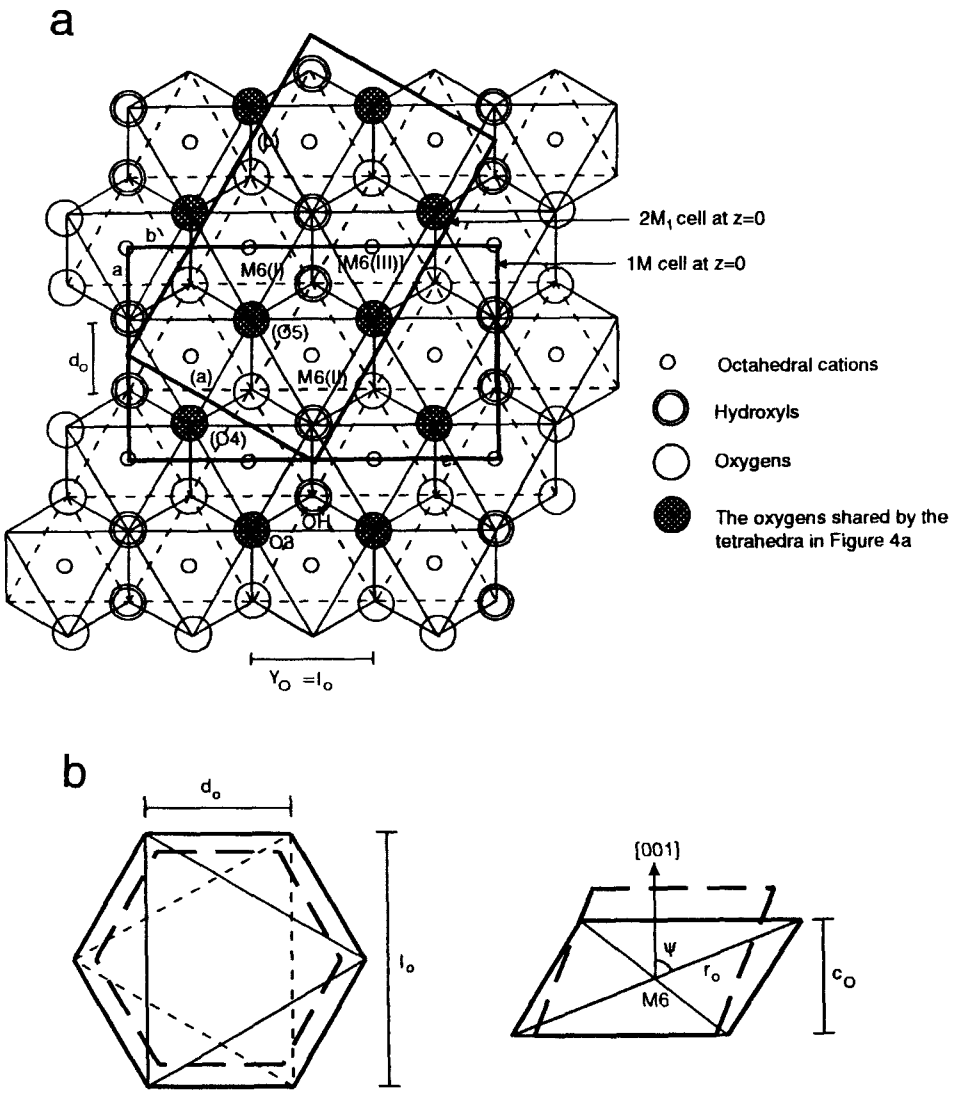

Fig. 3. Geometry of the atomic arrangement in the trioctahedral layer. a: Overall view of the atomic arrangement projected on (001). b: Octahedral flattening by an angle Ψ. The octahedra of broken and solid lines represent the octahedra before and after the flattening, respectively.

The shortest distance between the octahedral oxygen shared by the tetrahedra (Fig. 2a) becomes

$$Y_O=\sqrt{3}d_{oi}, \tag{16}$$

and the octahedral thicknesses (Fig. 2c) are given by

$$c_O=l_o'\cos(\eta-\xi_O), \text{ and} \tag{17}$$

$$c_H=l_o'\cos(\eta-\xi_H). \tag{18}$$

Trioctahedral Layer Structure Analyses

Fig. 3 shows the geometry of the atomic distribution in the trioctahedral layer. In contrast to the dioctahedral layer, the presence of an additional cation in site II results in equidirectional repulsion among the octahedral cations, and maintains oxygen distribution on (001) as a regular hexagon (Fig. 3a). However, the repulsion flattens the trioctahedral layer (Fig. 3b). Donnay et al. (1964) described the octahedral flattening with angle Ψ, expressed as

$$\Psi = a\sin\left(\frac{d_o}{r_o}\right), \tag{19}$$

where $d_o=d_{os}=d_{ol}=d_H=l_o/\sqrt{3}$, and r_o is obtained with equation (9). The octahedral edge length l_o (Fig. 3b) is given by

$$l_o = b/3. \tag{20}$$

The octahedral thickness becomes

$$c_O = 2r_o\cos(\Psi) \tag{21}$$

The thickness of the octahedral OH edge is empirically given by

$$c_H = c_O(1-0.01d(001)). \tag{22}$$

If substituted or vacant octahedral sites have an ordered configuration, the deformation of the octahedra is somewhat similar to that in the dioctahedral layer. For an ordered configuration of substituted or vacant octahedral sites, the projected longer and shorter octahedral edge lengths respectively become

$$d_{ol} = 2d_o\left(\frac{r_{o2}}{r_{o1}+r_{o2}}\right) \text{ and} \tag{23}$$

$$d_{os} = d_H = d_{ol}\left(\frac{r_{o1}}{r_{o2}}\right). \tag{24}$$

Fig. 3a shows that the shortest distance between the octahedral oxygen shared by the tetrahedra is also given by equation (16).

Tetrahedral Layer Structure Analyses

Random Tetrahedral Cation Configuration

Fig. 4 represents the geometry of the atomic arrangement in the tetrahedral layer with a random cation configuration. If the substitution of Al (or rarely Fe^{3+}) for Si in the tetrahedral sites is completely random, we may assume that all tetrahedra have the same average shape and size. If so, the average tetrahedral interatomic distance becomes

$$r_t = \sum_j f_{t,j} r_{t,j}. \tag{25}$$

See Table 2 for the values of $r_{t,j}$. For an ideal tetrahedron (Fig. 4b),

$$l_t = 2\sqrt{\frac{2}{3}}\, r_t. \tag{26}$$

For an ideal tetrahedral layer, the b-dimension becomes $2\sqrt{3}l_t$. However, this is usually larger than that of the octahedral layer. To compensate this size misfit, tetrahedra rotate by angle α (Fig. 4a) satisfying the following condition:

$$a = a\cos(l_a), \tag{27}$$

where

$$l_a = \frac{b}{2\sqrt{3}\,l_t}.$$

For most dioctahedral minerals or the trioctahedral minerals having ordered octahedral cation configurations, equation (27) usually overestimates the rotation angle. Neglecting the effect of tilting, which also reduces the b-dimension of the tetrahedral layer, causes the overestima-

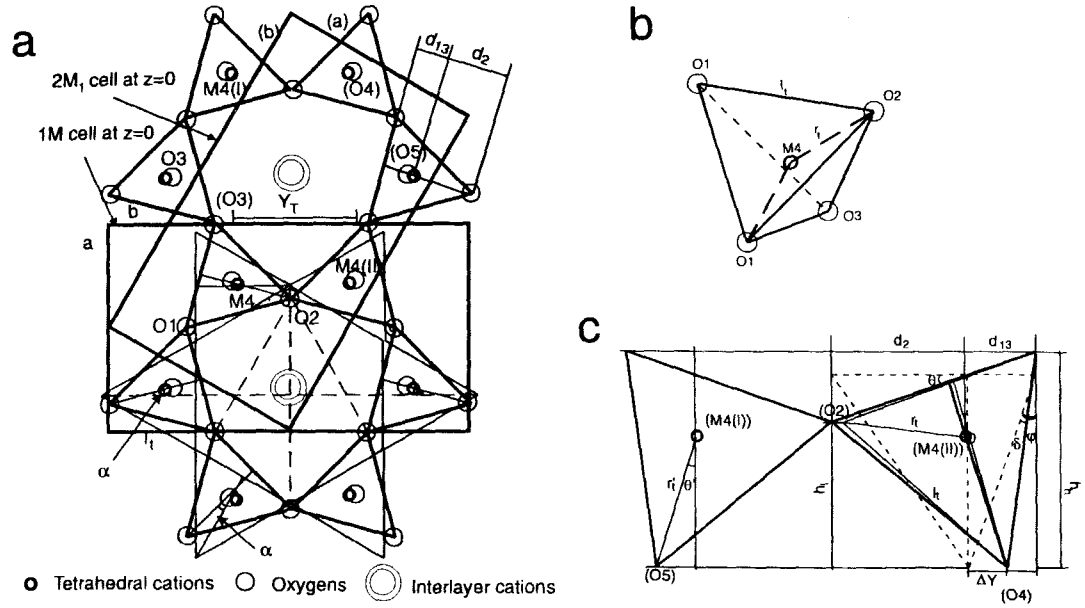

Fig. 4. Geometry of the atomic arrangement in the tetrahedral layer having a random tetrahedral cation configuration. a: Overall view of the atomic arrangement projected on (001). The thin and thick solid lines represent orientation of the tetrahedra before and after the rotation by an angle α, respectively. b: An ideal tetrahedron with edge length lt. c: The tetrahedral tilting by an angle δ. The tetrahedron with broken lines represents the tetrahedron before tilting. The tetrahedra of thin and thick solid lines represent tetrahedra before and after tetrahedral stretching after tilting, respectively.

tion. To reduce the overestimation of the rotation angle, l_a is empirically corrected to $l_a' = l_a/0.99$ for dioctahedral minerals and $l_a' = l_a/(1-0.01n_{[6]Al})$ for the trioctahedral minerals having ordered octahedral cation configurations. Then, the tetrahedral rotation angles for these minerals become

$$\alpha = a\cos(l_a'). \tag{28}$$

After the rotation of angle α, the shortest distance between the apical oxygen (Fig. 4a) becomes

$$Y_T = 2l_t\cos(\alpha)/\sqrt{3}. \tag{29}$$

The distance given by equation (29) must be equal to that by equation (16). Otherwise, the tetrahedra tilt to share the oxygen with the octahedra. Let

$$\Delta Y = \frac{Y_O - Y_T}{2\cos(\alpha)}, \tag{30}$$

which is the distance to be compensated by the tetrahedral tilting (Fig. 4c). Then, the tetrahedral tilting angle is given by

$$\delta = a\sin\left(\frac{l_t+\sqrt{3}\Delta Y}{\sqrt{3}l_t}\right) - a\sin\left(\frac{1}{\sqrt{3}}\right). \tag{31}$$

Due to the tilting, tetrahedra have two different heights, h_h and h_l (Fig. 4c);

$$h_l = l_t\cos\left(a\sin\left(\frac{l_t+\sqrt{3}\Delta Y}{\sqrt{3}l_t}\right)\right) \text{ and} \tag{32}$$

$$h_h = h_t + \frac{\sqrt{3}}{2} l_t \sin(\delta). \quad (33)$$

The tilting without tetrahedral deformation invokes the b-dimension mismatch. This study assumes that the bonding between the tetrahedral cation and the basal oxygens is stretched to maintain the b-dimension of the mineral (Fig. 4c). After the tetrahedral stretching, the tetrahedral cation should move to maintain its central occupancy in the tetrahedron. To describe the modified position of the tetrahedral cation, the apparent tilting angle (θ') and the distance between the tetrahedral cation and apical oxygen (r_t') must be known. Geometrical interpretation of the deformed tetrahedra should give following relations:

$$\theta = a\tan\left(\frac{l_t/(2\sqrt{3}) - \sqrt{3}\, l_t \sin(\varphi - \delta)/2}{h_h - l_t \tan\theta/(2\sqrt{3})}\right), \quad (34)$$

where

$$\theta = a\tan(\sin(\delta)), \text{ and } \varphi = a\sin\left(\frac{1}{3}\right).$$

$$r_t' = \frac{3}{4\cos\theta}\left(h_h - \frac{l_t \tan\theta}{2\sqrt{3}}\right). \quad (35)$$

With θ' and r_t' from equations (34) and (35), d_{13} and d_2 in Fig. 4c can be calculated:

$$d_{13} = \frac{l_t}{2\sqrt{3}} - \frac{r_t'}{3}\sin(\theta), \text{ and} \quad (36)$$

$$d_2 = \frac{l_t}{\sqrt{3}} + \frac{r_t'}{3}\sin(\theta). \quad (37)$$

Ordered Tetrahedral Cation Configuration

Fig. 5 represents the geometry of the atomic arrangements in the tetrahedral layer with an ordered cation configuration. This study allows only cation ordering between sites I and II to maintain C2 or C2/c symmetry. The method of most structural refinement of the tetrahedral layer with an ordered cation configuration is similar to the refinement of the layers with random cation configurations, but separate calculations of the average tetrahedral interatomic distances, edge lengths, and tilting angles are necessary due to two different sizes of the tetrahedra of sites I and II.

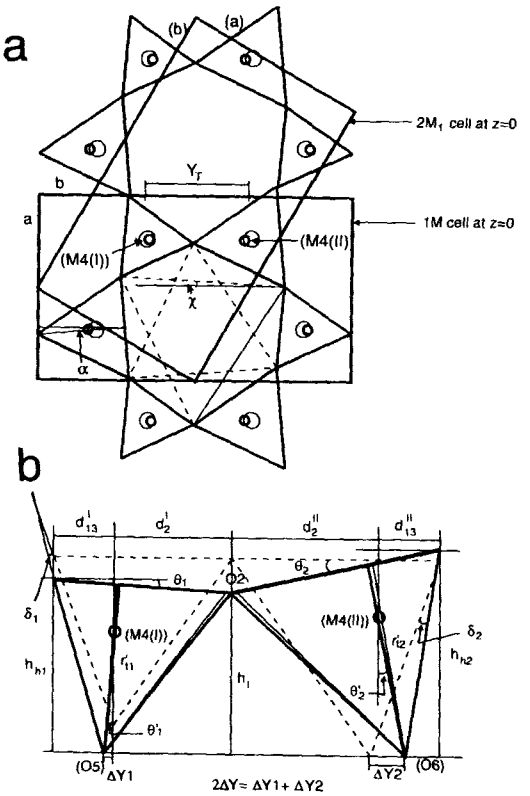

Fig. 5. Geometry of the atomic arrangement in the tetrahedral layer having an ordered tetrahedral cation configuration. a: Overall view of the atomic arrangement projected on (001). The positions of the basal oxygens and interlayer cations are not depicted. b: Tetrahedral tilting by angles δ1 and δ2. The tetrahedra with broken lines represent tetrahedra before tilting. The tetrahedra of thin and thick solid lines represent tetrahedra before and after tetrahedral stretching after tilting, respectively.

The average bond lengths of sites I and II

respectively become

$$r_{t1} = \sum_j f_{t1,j} r_{t,j} \text{ and} \quad (38)$$

$$r_{t2} = \sum_j f_{t2,j} r_{t,j}. \quad (39)$$

The edge lengths, l_{t1} and l_{t2}, of the tetrahedra of sites I and II can be calculated using equation (26). The rotation angle of the tetrahedra is given by equation (27) or (28), but Fig. 5a indicates that the argument of equation (27) must be replaced with

$$l_a = \frac{b}{\sqrt{3}(l_{t1} + l_{t2})}.$$

The distance compensated by the tetrahedral tilting is also defined by equation (30), but YT in equation (30) must be modified to

$$Y_T = \frac{(l_{t1} + l_{t2})\cos(a)}{\sqrt{3}}. \quad (40)$$

The tetrahedra of sites I and II must tilt to share O2 and compensate the distance ΔY, satisfying the following two conditions (Fig. 5b):

$$l_{t1}\cos(\varepsilon + \delta_1) = l_{t2}\cos(\varepsilon + \delta_2) \text{ and} \quad (41)$$

$$l_{t1}(\sin(\varepsilon + \delta_1) - \sin(\varepsilon)) + l_{t2}(\sin(\varepsilon + \delta_2) - \sin(\varepsilon)) = 2\Delta Y, \quad (42)$$

where

$$\varepsilon = a\sin\left(\frac{1}{3}\right).$$

Iterative calculations of equations (41) and (42) give δ_1 and δ_2. As a result of the tilting, tetrahedra of sites I and II should have the same lower height given by

$$h_l = l_{t1}\cos(\varepsilon + \delta_1). \quad (43)$$

However, the tetrahedra of sites I and II should have two different higher heights (Fig. 5b);

$$h_{h1} = h_l + \frac{\sqrt{3}}{2} l_{t1}\sin(\delta_1) \text{ and}$$

$$h_{h2} = h_l + \frac{\sqrt{3}}{2} l_{t2}\sin(\delta_2).$$

The different heights of the tetrahedra of sites I and II destroy C2 or C2/c symmetry of the mineral. Thus, the phyllosilicates having an ordered tetrahedral cation configuration can not have C2 or C2/c symmetry without further tetrahedral deformation. It is believed that this is the case for naturally occurring phyllosilicates having an ordered tetrahedral cation configuration (Guggenheim and Bailey, 1975). To maintain C2 or C2/c symmetry of the mineral, PHYLS assumes that the tetrahedra deform to have the same higher height, given by

$$h_h = \frac{h_{h1} + h_{h2}}{2}. \quad (44)$$

The tetrahedral tilting causes tetrahedral stretching described with the apparent tilting angles and the distances between the tetrahedral cation and the apical oxygen at sites I and II. Those parameters are given by

$$\theta_1' = a\tan\left(\frac{l_{t1}/(2\sqrt{3}) - \sqrt{3}\, l_{t1}\sin(\varphi - \delta_1)/2}{h_h - l_{t1}\tan\theta_1/(2\sqrt{3})}\right)$$

and (45)

$$\theta_2' = a\tan\left(\frac{l_{t2}/(2\sqrt{3}) - \sqrt{3}\, l_{t2}\sin(\varphi - \delta_2)/2}{h_h - l_{t2}\tan\theta_2/(2\sqrt{3})}\right), \quad (46)$$

where

$$\theta_1 = a\tan(\sin(\delta_1)),$$

$$\theta_2 = a\tan(\sin(\delta_2)), \text{ and}$$

$$\varphi = a\sin\left(\frac{1}{3}\right).$$

$$r_{t2}' = \frac{3}{4\cos\theta_1}\left(h_h - \frac{l_{t1}\tan\theta_1}{2\sqrt{3}}\right) \text{ and} \quad (47)$$

$$r_{t2}' = \frac{3}{4\cos\theta_2}\left(h_h - \frac{l_{t2}\tan\theta_2}{2\sqrt{3}}\right). \quad (48)$$

With θ_1', θ_2', r_{t1}', and r_{t2}' from equations (45) to (48), d_{13}^{I}, d_{13}^{II}, d_2^{I}, and d_2^{II} in Fig. 5b can be similarly calculated to the equations (36) and (37);

$$d_{13}^{I} = \frac{l_{t1}}{2\sqrt{3}} - \frac{r_{t1}'}{3}\sin(\theta_1'), \quad (49)$$

$$d_{13}^{II} = \frac{l_{t2}}{2\sqrt{3}} - \frac{r_{t2}'}{3}\sin(\theta_2'), \quad (50)$$

$$d_{12}^{I} = \frac{l_{t1}}{\sqrt{3}} + \frac{r_{t1}'}{3}\sin(\theta_1'), \text{ and} \quad (51)$$

$$d_{12}^{II} = \frac{l_{t2}}{\sqrt{3}} + \frac{r_{t2}'}{3}\sin(\theta_2'). \quad (52)$$

Interlayer Structure Analyses

Random Tetrahedral Cation Configuration

The tetrahedral tilting shifts the interlayer cation to the position of O2 from the center of the inner triad of the basal oxygens in Fig. 4a. Fig. 6 depicts how the interlayer cation is shifted. The shift distance can be calculated with

$$d_i = \left(\frac{d(001) - c_O - 2h_l}{2} - \frac{2(h_h - h_l)}{3}\right)\left(\frac{h_h - h_l}{\sqrt{3}\,l_t\sin(60° - \alpha)}\right). \quad (53)$$

Then, the interaxial angle becomes

$$\beta = 90° + a\tan\left(\frac{l_{ol} + 2d_i}{d(001)}\right). \quad (54)$$

The average interatomic distance between the interlayer cation and the basal oxygens comprising the inner triad is given by

$$r_i = \sqrt{\left(\frac{d(001) - c_o - 2h_l}{2}\right)^2 + \left(\frac{2q}{3} - d_i\right)^2}, \quad (55)$$

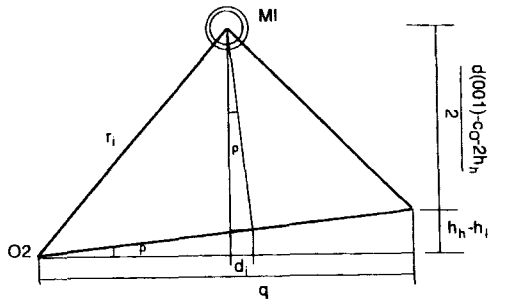

Fig. 6. Schematic representation of the interlayer cation shift, viewed along the direction of a-axis of a 1M unit cell.

where

$$q = \sqrt{3}\,l_t\sin(60° - \alpha).$$

Ordered Tetrahedral Cation Configuration

Due to the different sizes of the tetrahedra of sites I and II, the direction of the interlayer cation shift rotates toward the smaller tetrahedron from the direction for a random tetrahedral cation configuration (Fig. 5a). The rotation angle, x, is given by

$$\chi = a\tan\left(\frac{(l_{t1} - l_{t2})\sin(30° - \alpha)}{(l_{t1} + l_{t2})\cos(30° - \alpha)}\right). \quad (56)$$

The distance of the interlayer cation shift is similarly given to equation (53);

$$d_i = \left(\frac{d(001) - c_O - 2h_l}{2} - \frac{2(h_h - h_l)}{3}\right)\left(\frac{2(h_h - h_l)}{\sqrt{3}(l_{t1} + l_{t2})\sin(60° - \alpha)}\right). \quad (57)$$

Then, the interaxial angle become

$$\beta = 90° + a\tan\left(\frac{l_{ol} + 2d_i\cos(\chi)}{d(001)}\right). \quad (58)$$

The interatomic distance is also given by

Table 3. Atomic coordinate calculation for 1M phyllosilicates having a random tetrahedral cation configuration and space group C2/m.

Sites	x	y	z
M6(I)	0	1/3	0
M6(II)*	1/2	1/2	0
O3	$\frac{d_{os}+d_{ol}}{2a}-z_{O3}\cos(\beta)\frac{c}{a}$	$\frac{\sqrt{3}(d_{os}+d_{ol})}{2b}$	$\frac{c_o}{2d(001)}$
OH	$0.5-\frac{d_H}{2a}-z_{OH}\cos(\beta)\frac{c}{a}$	0	$\frac{c_{OH}}{2d(001)}$
M4	$x_{O3}+\frac{r_t'\sin(\theta')\sin(\alpha)}{a}$ $-(z_{M4}-z_{O3})\cos(\beta)\frac{c}{a}$	$y_{O3}+\frac{r_t'\sin(\theta')\cos(\alpha)}{b}$	$z_{O3}+\frac{r_t'\cos(\theta')}{d(001)}$
O1	$x_{M1}+\frac{l_t\cos(\alpha)}{2a}-\frac{d_{13}\sin(\alpha)}{a}$ $-(z_{O1}-z_{M1})\cos(\beta)\frac{c}{a}$	$y_{M1}+\frac{l_t\sin(\alpha)}{2b}-\frac{d_{13}\cos(\alpha)}{b}$	$z_{O3}+\frac{h_h}{d(001)}$
O2	$x_{M1}+\frac{d_2\sin(\alpha)}{a}$ $-(z_{O2}-z_{M1})\cos(\beta)\frac{c}{a}$	1/2	$z_{O3}+\frac{h_t}{d(001)}$
MI	0	1/2	1/2

*: For trioctahedral phyllosilicates only.

equation (55), but q in the equation must be replaced with

$$q=\frac{\sqrt{3}}{2}(l_{t1}+l_{t2})\sin(60^\circ-\alpha).$$

Coordinates Calculation

Given the above geometrical relations among the constituent atoms, as shown in Figs 3, 4, 5, and 6, the atomic coordinates of the crystallographically independent sites of the 2:1 dioctahedral phyllosilicates in space groups C2/m, C2, and C2/c may be calculated. Tables 3, 4, 5, and 6 summarize the formulations of the atomic coordinates in terms of the distances and angles obtained by geometrical structural analyses.

Program Output

The output from PHYLS consists of the atomic coordinates, cell dimensions, interaxial angle, β, deformation angles, bond lengths, and cell volume of the mineral. A sample output is presented in Appendix III.

RESULTS AND DISCUSSION

Table 7 compares the predicted structures of $2M_1$ dioctahedral micas by PHYLS with reported experimentally determined structures, having a random tetrahedral cation configura-

Table 4. Atomic coordinate calculation for 1M phyllosilicates having an ordered tetrahedral cation configuration and space group C2.

Sites	x	y	z
M6(I)	0	1/3	0
M6(II)	0	2/3	0
M6(III)*	1/2	1/2	0
O4	$\frac{d_{os}+d_{ol}}{2a}-z_{O4}\cos(\beta)\frac{c}{a}$	$\frac{\sqrt{3}(d_{os}+d_{ol})}{2b}$	$\frac{c_o}{2d(001)}$
O5	x_{O4}	$-y_{O4}$	z_{O4}
OH	$-\frac{d_H}{2a}-z_{OH}\cos(\beta)\frac{c}{a}$	0	$\frac{c_{OH}}{2d(001)}$
M4(I)	$x_{O5}+\frac{r_{t1}'\sin(\theta_1')\sin(\alpha)}{a}$ $-(z_{M4(I)}-z_{O5})\cos(\beta)\frac{c}{a}$	$y_{O5}-\frac{r_{t1}'\sin(\theta_1')\cos(\alpha)}{b}$	$z_{O5}+\frac{r_{t1}'\cos(\theta_1')}{d(001)}$
M4(II)	$x_{O4}+\frac{r_{t2}'\sin(\theta_2')\sin(\alpha)}{a}$ $-(z_{M4(II)}-z_{O4})\cos(\beta)\frac{c}{a}$	$y_{O4}+\frac{r_{t2}'\sin(\theta^{2'})\cos(\alpha)}{b}$	$z_{O4}+\frac{r_{t2}'\cos(\theta_2')}{d(001)}$
O1	$x_{M4(I)}+\frac{l_{t1}\cos(\alpha)}{2a}-\frac{d_{13}^I\sin(\alpha)}{a}$ $-(z_{O1}-z_{M4(I)})\cos(\beta)\frac{c}{a}$	$y_{M4(I)}-\frac{l_{t1}\sin(\alpha)}{2b}-\frac{d_{13}^I\cos(\alpha)}{b}$	$z_{O4}+\frac{h_h}{d(001)}$
O2	$x_{M4(I)}+\frac{d_2^I\sin(\alpha)}{a}$ $-(z_{O2}-z_{M4(I)})\cos(\beta)\frac{c}{a}$	1/2	$z_{O4}+\frac{h_l}{d(001)}$
O3	$x_{M4(I)}-\frac{l_{t1}\cos(\alpha)}{2a}-\frac{d_{13}^I\sin(\alpha)}{a}$ $-(z_{O3}-z_{M4(I)})\cos(\beta)\frac{c}{a}$	$y_{M4(I)}+\frac{l_{t1}\sin(\alpha)}{2b}-\frac{d_{13}^I\cos(\alpha)}{b}$	z_{O1}
MI	0	1/2	1/2

*: For trioctahedral phyllosilicates only.

tion. Overall, the differences between the predicted and reported values in Table 7 indicate that the PHYLS can simulate mica structures closely to the reported ones. However, there are a few predicted structural parameters showing significant differences between calculation and experiment. The predicted y-coordinate of MI shows a relatively large deviation from the reported value, suggesting that d_i is overestimated. The overestimation of d_i is due to the overestimation of δ (see the z-coordinate difference of O2), which in turn causes the overestimation of β and more or less large difference in the x-coordinates of such structural

Table 5. Atomic coordinate calculation for $2M_1$ phyllosilicates having a random tetrahedral cation configuration and space group C2/c.

Sites	x	y	z
M6(I)	1/4	1/12	0
M6(II)*	3/4	1/4	0
O4	$\frac{(d_{os}/4+d_{ol})}{a}-z_{O4}\cos(\beta)\frac{c}{a}$	$-\frac{\sqrt{3}d_{os}}{4b}$	$\frac{c_o}{2d(001)}$
O5	$\frac{(3d_{os}/4+d_{ol}/2)}{a}-z_{O5}\cos(\beta)\frac{c}{a}$	$\frac{\sqrt{3}}{2b}\left(\frac{d_{os}}{2}+d_{ol}\right)$	z_{O4}
OH	$-\frac{d_H}{4a}-z_{OH}\cos(\beta)\frac{c}{a}$	$\frac{\sqrt{3}d_H}{4b}$	$\frac{c_{OH}}{2d(001)}$
M4(I)	$x_{O5}+\frac{r_t'\sin(\theta')\cos(30°-\alpha)}{a}$ $-(z_{M4(I)}-z_{O5})\cos(\beta)\frac{c}{a}$	$y_{O5}+\frac{r_t'\sin(\theta')\sin(30°-\alpha)}{b}$	$z_{O5}+\frac{r_t'\cos(\theta')}{d(001)}$
M4(II)	$x_{O4}-\frac{r_t'\sin(\theta')\cos(30°-\alpha)}{a}$ $-(z_{M4(II)}-z_{O4})\cos(\beta)\frac{c}{a}$	$y_{O4}-\frac{r_t'\sin(\theta')\sin(30°+\alpha)}{b}$	$z_{O4}+\frac{r_t'\cos(\theta')}{d(001)}$
O1	$x_{M4(II)}-\frac{l_t\sin(30°+\alpha)}{2a}$ $+\frac{d_{13}\sin(60°-\alpha)}{a}$ $-(z_{O1}-z_{M4(II)})\cos(\beta)\frac{c}{a}$	$y_{M4(II)}+\frac{l_t\cos(30°+\alpha)}{2b}$ $+\frac{d_{13}\cos(60°-\alpha)}{b}$	$z_{O4}+\frac{h_h}{d(001)}$
O2	$x_{M4(II)}-\frac{d_2\sin(60°-\alpha)}{a}$ $-(z_{O2}-z_{M4(II)})\cos(\beta)\frac{c}{a}$	$y_{M4(II)}-\frac{d_2\cos(60°-\alpha)}{b}$	$z_{O4}+\frac{h_l}{d(001)}$
O3	$x_{M4(II)}+\frac{l_t\cos(60°-\alpha)}{2a}$ $+\frac{d_{13}\sin(60°-\alpha)}{a}$ $-(z_{O3}-z_{M4(II)})\cos(\beta)\frac{c}{a}$	$y_{M4(II)}-\frac{l_t\sin(60°-\alpha)}{2b}$ $+\frac{d_{13}\cos(60°-\alpha)}{b}$	z_{O1}
MI	$-\frac{d_{ol}/2+d_i}{2a}-z_{MI}\cos(\beta)\frac{c}{a}$	$\left(\frac{d_{ol}}{2}+d_i\right)\frac{\sqrt{3}}{2b}$	1/4

*: For trioctahedral phyllosilicates only.

sites as M4(I) and O3. To reduce these errors, one may need to add some empirical corrections to the simple geometrical calculation of δ of this study.

Even after the empirical correction of δ, the structure prediction might be little improved due to poor experimental data. The most significant source of error is the chemical composition

Table 6. Atomic coordinate calculation for $2M_1$ phyllosilicates having an ordered tetrahedral cation configuration and space group C2/c.

Sites	x	y	z
The coordinate calculations for M6(I), M6(II), O4, O5, and OH are the same as in Table 5.			
M4(I)	$x_{O5}+\frac{r_{t1}'\sin(\theta_1')\cos(30°-\alpha)}{a}$ $-(z_{M4(I)}-z_{O5})\cos(\beta)\frac{c}{a}$	$y_{O5}+\frac{r_{t1}'\sin(\theta_1')\sin(30°-\alpha)}{b}$	$z_{O5}+\frac{r_{t1}'\cos(\theta_1')}{d(001)}$
M4(II)	$x_{O4}-\frac{r_{t2}'\sin(\theta_2')\sin(60°-\alpha)}{a}$ $-(z_{M4(II)}-z_{O4})\cos(\beta)\frac{c}{a}$	$y_{O4}-\frac{r_{t2}'\sin(\theta_2')\sin(60°-\alpha)}{b}$	$z_{O4}+\frac{r_{t2}'\cos(\theta_2')}{d(001)}$
O1	$x_{M4(II)}-\frac{l_{t2}\sin(30°+\alpha)}{2a}$ $+\frac{d_{13}^{II}\sin(60°-\alpha)}{a}$ $-(z_{O1}-z_{M4(II)})\cos(\beta)\frac{c}{a}$	$y_{M4(II)}+\frac{l_{t2}\cos(30°+\alpha)}{2b}$ $+\frac{d_{13}^{II}\cos(60°-\alpha)}{b}$	$z_{O4}+\frac{h_h}{d(001)}$
O2	$x_{M4(II)}-\frac{d_2^{II}\sin(60°-\alpha)}{a}$ $-(z_{O2}-z_{M4(II)})\cos(\beta)\frac{c}{a}$	$y_{M4(II)}-\frac{d_2^{II}\cos(60°-\alpha)}{b}$	$z_{O4}+\frac{h_l}{d(001)}$
O3	$x_{M4(II)}+\frac{l_{t2}\cos(60°-\alpha)}{2a}$ $+\frac{d_{13}^{II}\sin(60°-\alpha)}{a}$ $-(z_{O3}-z_{M4(II)})\cos(\beta)\frac{c}{a}$	$y_{M4(II)}-\frac{l_{t2}\sin(60°-\alpha)}{2b}$ $+\frac{d_{13}^{II}\cos(60°-\alpha)}{b}$	z_{O1}
MI($l_{t1}<l_{t2}$)	$-\frac{d_{ol}/4+d_i\sin(30°+\chi)}{a}$ $-z_{MI}\cos(\beta)\frac{c}{a}$	$-\frac{\sqrt{3}d_{ol}/4+d_i\cos(30°+\chi)}{b}$	1/4
MI($l_{t1}<l_{t2}$)	$-\frac{d_{ol}/4+d_i\sin(30°-\chi)}{a}$ $-z_{MI}\cos(\beta)\frac{c}{a}$	$-\frac{\sqrt{3}d_{ol}/4+d_i\cos(30°-\chi)}{b}$	1/4

*: For trioctahedral phyllosilicates only.

of the mineral. The chemical compositions of phyllosilicates are often incomplete and inaccurate. For example, the chemical composition of the muscovite in Table 7 indicates that charge neutrality is not satisfied. Incorrect input of the chemical composition causes incorrect calculation of the b-dimension, interatomic distances, and all the other structural parameters.

Table 8 shows the results of the structure prediction of 2:1 phyllosilicates having ordered tetrahedral cation configuration. As mentioned previously, the ordering of the cations in the tetrahedral sites probably prevents the mineral from having space groups of C2 or C2/c.

Table 7. Comparison of PHYLS-predicted structures of $2M_1$ dioctahedral micas having random tetrahedral cation configurations with experimentally determined structures.

Muscovite (Gven, 1971)

Data: chemical composition=$(K_{.86}Na_{.1})(Al_{1.9}Fe^{3+}_{.02}Fe^{2+}_{.05}Mg_{.06})(Al_{.98}Si_{3.02})O_{10}(OH)_2$, d(002)=9.973 Å, space group=C2/c, cation configuration=random

	Predicted	Δ*		Predicted			Δ		
				x	y	z	x	y	z
a	5.1942 Å	0.0036 Å	MI	.0000	.1104	.2500	-	.0119	-
b	8.9967 Å	-0.0113 Å	M6	.2500	.0833	.0000	.0004	-.0001	-
c	20.0774 Å	-0.0304 Å	M4(I)	.9768	.4303	.1353	.0120	.0008	-.0002
b	96.558°	0.801°	M4(II)	.4558	.2566	.1353	.0048	-.0018	-.0002
V	932.10 $Å^3$	-0.51 $Å^3$	O1	.4190	.0938	.1671	.0016	.0008	-.0014
ro	1.928 Å	0.004 Å	O2	.7545	.3100	.1537	.0032	-.0010	-.0038
rt	1.643 Å	-	O3	.2655	.3726	.1671	.0133	.0021	-.0018
ri	2.893 Å	-0.038 Å	O4	.9683	.4447	.0535	.0070	.0012	-.0005
a	12.12°	0.77°	O5	.3843	.2500	.0535	-.0007	-.0019	-.0002
d	6.61°	NA**	OH	.9577	.0646	.0506	.0013	.0016	.0001
w	6.05°	NA							

Phengite (Gven, 1971)

Data: Chemical composition=$(K_{.87}Na_{.07}Ca_{.02})(Al_{1.43}Fe^{3+}_{.05}Fe^{2+}_{.09}Mg_{0.5})(Al_{.61}Si_{3.39})O_{10}(OH)_2$, d(002)=9.923 Å, space group=C2/c, cation configuration=random

	Predicted	Δ		Predicted			Δ		
				x	y	z	x	y	z
a	5.2075 Å	-0.0037 Å	MI	.0000	.1053	.2500	-	.0089	-
b	9.0196 Å	-0.0187 Å	M6	.2500	.0833	.0000	.0033	-.0008	-
c	19.9669 Å	0.0196 Å	M4(I)	.9744	.4293	.1371	.0112	-.0006	-.0016
b	96.308°	0.539°	M4(II)	.4554	.2564	.1371	.0029	-.0017	-.0017
V	932.16 $Å^3$	-2.61 $Å^3$	O1	.4334	.0940	.1680	-.0092	.0009	.0002
ro	1.962 Å	0.006 Å	O2	.7454	.3184	.1569	.0082	-.0073	-.0032
rt	1.631 Å	0.003 Å	O3	.2551	.3645	.1680	.0225	.0071	-.0002
ri	2.939 Å	-0.031 Å	O4	.9637	.4404	.0553	.0065	.0008	.0009
a	8.99°	2.94°	O5	.3924	.2500	.0553	-.0009	-.0004	-.0016
d	5.51°	NA	OH	.9547	.0675	.0527	.0016	.0019	.0001
w	5.03°	NA							

*Δ=predicted value minus reported value.

** NA=not available.

Thus, the predicted structure in Table 8 must be approximate, and the differences between the predicted and reported ones are more significant than in the case of random tetrahedral

Table 8. Comparison of PHYLS-predicted structures of 2M1 margarite and 1M dioctahedral mica having ordered tetrahedral cation configurations with experimentally determined structures.

Margarite (Takeuchi, 1965)

Data: chemical composition=$(K_{.009}Na_{.19}Ca_{.812})(Al_{1.992}Fe^{2+}_{.012}Mg_{0.032})(Al_{1.89}Si_{2.11})O_{10}(OH)_2$,
d(002)=9.566 Å, space group=C2/c, cation configuration=ordered, $f_{t1,Si}$=1.0, $f_{t2,Al}$=1.0

	Predicted	Δ*		Predicted			Δ		
				x	y	z	x	y	z
a	5.1427 Å	0.0197 Å	MI	.0000	.0998	.2500	-	.0056	-
b	8.9073 Å	0.0213 Å	M6	.2500	.0833	.0000	-.0018	.0018	-
c	19.2418 Å	0.0208 Å	M4(I)	.4401	.2522	.1429	-.0142	-.0053	-.0009
β	96.125°	0.625°	M4(II)	.4650	.9201	.1429	.0022	-.0082	-.0003
V	876.38 $Å^3$	5.43 $Å^3$	O1	.3651	.0876	.1764	.0054	-.0008	-.0024
r_o	1.921 Å	0.009 Å	O2	.2496	.7741	.1630	-.0290	-.0098	-.0065
r_{t1}	1.610 Å	-0.082 Å	O3	.2803	.3758	.1764	.0103	-.0145	-.0033
r_{t2}	1.745 Å	0.043 Å	O4	.9651	.4429	.0558	.0104	-.0001	.0005
r_i	2.144 Å	-0.314 Å	O5	.3866	.2500	.0558	-.0008	-.0024	-.0011
α	18.53°	-1.87°	OH	.4553	.5659	.0530	.0061	.0035	.0025
δ_1	3.47°	NA**							
δ_2	8.71°	NA							
ω	5.61°	NA							

1M mica (Sidorenko et al., 1975)

Data: chemical composition=$(K_{.65}Na_{.03})(Al_{1.83}Fe^{2+}_{.03}Fe^{2+}_{.035}Mg_{0.1})(Al_{.49}Si_{3.51})O_{10}(OH)_2$,
d(001)=9.905 Å, space group=C2, cation configuration=ordered,
$f_{t1,Si}$=0.96, $f_{t1,Al}$=0.04, $f_{t1,Si}$=0.83, $f_{t2,Al}$=0.17

	Predicted	Δ		Predicted			Δ		
				x	y	z	x	y	z
a	5.2029 Å	0.0169 Å	MI	.0000	.5000	.5000	-	-.0008	-
b	9.0117 Å	0.0597 Å	M6(I)	.0000	.3333	.0000	-	-.0045	-
c	10.1632 Å	0.0432 Å	M6(II)	.0000	.6667	.0000	-	-.0052	-
β	102.943°	1.110°	M4(I)	.4286	.3251	.2709	.0079	-.0039	.0019
V	464.41 $Å^3$	4.57 $Å^3$	M4(II)	.4292	.6724	.2709	.0104	.0005	.0012
r_o	1.932 Å	-0.008 Å	O1	.1891	.7281	.3340	.0091	-.0021	.0032
r_{t1}	1.615 Å	0.001 Å	O2	.4859	.5000	.3074	.0018	-.0003	-.0087
r_{t2}	1.633 Å	-0.001 Å	O3	.1868	.2678	.3340	.0234	-.0106	-.0044
r_i	2.984 Å	0.087 Å	O4	.3527	.3054	.1080	.0042	-.0102	-.0002
α	7.80°	-1.60°	O5	.3527	.6946	.1080	.0051	-.0023	.0010
δ_1	6.25°	NA	OH	.4153	.5000	.1021	-.0092	-.0141	-.0027
δ_2	6.94°	NA							
ω	6.03°	-0.87°							

*Δ=predicted value minus reported value.
** NA=not available.

Table 9. Comparison of PHYLS-predicted structures of 1M trioctahedral micas having random tetrahedral cation configurations with experimentally determined structures.

Phlogopite (Hazen and Burnham, 1973)

Data: chemical composition=$(K_{.77}Na_{.16})(Mg_{3.0})(Al_{1.05}Si_{2.95})O_{10}(OH)_2$,
d(001)=9.998 Å, space group=C2/m, cation configuration=random

	Predicted	Δ*		Predicted			Δ		
				x	y	z	x	y	z
a	5.3174 Å	0.0096 Å	MI	.0000	.0000	.0000			-
b	9.2100 Å	-0.0199 Å	M6(I)	.0000	.1667	.5000			-
c	10.1539 Å	-0.0008 Å	M6(II)	.0000	.5000	.5000	-	-	-
β	100.053°	-0.027°	M4	.5779	.1667	.2306	-	-.0018	.0052
V	489.63 Å^3	1.93 Å^3	O1	.8287	.2299	.1758	-	-	.0081
r_o	2.060 Å	-0.004 Å	O2	.5185	.0000	.1758	.0027	-.0001	.0083
r_t	1.644 Å	-0.005 Å	O3	.6317	.1667	.3950	.0039	-.0008	.0048
r_i	3.012 Å	0.043 Å	OH	.1352	.0000	.4055	.0005	-	.0047
α	7.91°	0.41°					.0002	.0003	
δ	0.0°	-					.0022	-	
ψ	59.36°	0.40°							

Annite (Hazen and Burnham, 1973)

Data: chemical composition=$(K_{.88}Na_{.07}Ca_{.03})(Al_{.09}Fe^{3+}_{.19}Fe^{2+}_{2.6}Mg_{.12})(Al_{1.19}Si_{2.81})O_{10}(OH)_2$,
d(001)=10.092 Å, space group=C2/m, cation configuration=random

	Predicted	Δ		Predicted			Δ		
				x	y	z	x	y	z
a	5.3911 Å	0.0051 Å	MI	.0000	.0000	.0000	-	-	-
b	9.3377 Å	0.1360 Å	M6(I)	.0000	.1667	.5000	-	-.0001	-
c	10.2507 Å	-0.0176 Å	M6(II)	.0000	.5000	.5000	-	-	-
β	100.097°	-0.533°	M4	.5754	.1667	.2264	.0051	.0002	.0010
V	508.04 Å^3	1.24 Å^3	O1	.8073	.2500	.1718	.0042	.0003	.0048
r_o	2.113 Å	0.012 Å	O2	.5573	.0000	.1718	.0146	-	.0034
r_t	1.651 Å	-0.008 Å	O3	.6300	.1667	.3899	.0009	-.0007	.0005
r_i	3.205 Å	0.061 Å	OH	.1337	.0000	.4010	.0098	-	.0079
α	0.00°	-1.5°							
δ	0.00°	-							
ψ	58.28°	0.08°							

*Δ=predicted value minus reported value.

cation configurations. The structure of margarite in Table 8 is predicted by assuming a perfect ordering of the tetrahedral cations and compared to the structure of Takeuchi (1965) having C2/c symmetry. Although the predicted margarite structure is comparable with Takeuchi's structure,

Guggenheim and Bailey (1975) later found from refinement of the margarite structure that the mineral has Cc symmetry, due to tetrahedral cation ordering. Guggenheim and Bailey's symmetry of margarite is pertinent to the geometrical analysis described earlier in this study. Assuming C2 symmetry and partial ordering of the tetrahedral cations, the structure of 1M dioctahedral mica, probably representing illite, is predicted and compared with the structure of Sidorenko et al. (1975) in Table 8. Because of the small difference in Al contents among the tetrahedral sites in 1M mica, its structure prediction agrees much better with the experimental structure than the margarite structure prediction agrees with its experimental counterpart. The predicted structures of the phyllosilicates having partially ordered tetrahedral cation configuration may be useful in structural property related studies and in energy minimization refinements.

Table 9 summarized the predicted 1M trioctahedral mica structures, compared with experimental structures of Hazen and Burnham (1973). The differences between the predicted and reported structural values in Table 9 indicate that the geometrical prediction of 1M trioctahedral mica structure is excellent. All the predicted z-coordinates show small positive errors, indicating that Ψ is slightly overestimated. Using $\Psi/0.975$ instead of the calculated Ψ improves the prediction of the z-coordinates with insignificant influence on the prediction of x- and y-coordinates. However, we recommend PHYLS use an unmodified Ψ, as much as possible to eliminate empirical corrections.

SUMMARY

FORTRAN program PHYLS geometrically predicts the structures of 2:1 dioctahedral and trioctahedral phyllosilicates having space groups C2/m, C2, and C2/c. PHYLS predicts the structures of 1M and $2M_1$ phyllosilicates close to the reported ones, whether they are dioctahedral or trioctahedral, when the tetrahedral cations distribute randomly. On the other hand, the predicted structures of the minerals having ordered tetrahedral cation configurations deviate from the reported ones due to the large difference in size of the tetrahedral sites. However, if the ordering of the tetrahedral cations is partial, so that the size difference between the tetrahedral sites is not large, the predicted structures are sufficiently accurate to be used to determine structural and thermodynamic properties.

PHYLS may be improved to predict more accurate structural parameters and atomic arrangements in the future. Other regression equations predicting the b-dimension may be used to describe the relationship between structure and chemical composition more accurately. The tetrahedral rotation and tilting angles may be solved simultaneously, although the solution requires non-linear optimization and iteration programming. An empirical correction to the estimation of the tilting angle may be necessary, then all the related structural parameters can be recalculated with respect to the corrected tilting angle. Other empirical corrections can also be adapted in the structural parameter calculation to finely adjust the predicted structures to the reported ones. However, we reiterate that errors in the reported chemical analyses may cause significant parameter differences, when comparing predicted structures with experimentally determined structures. Finally, PHYLS will need additions to calculate structures of polytypes 3T, 2Or, 6H and 2M2 and symmetries

Cc, $P3_112$ and Cm.

NOTATION

a, b, c cell-dimensions

c_O thickness of octahedral layer along [001]

c_H thickness of octahedral OH-OH edge along [001]

d_t interlayer cation shift due to tetrahedral tilting

d_{ol} long octahedral edge length projected on (001)

d_{os} short octahedral edge length projected on (001)

d_{13} distance between the tetrahedral cation and the midpoint of the line connecting the basal oxygens O1 and O3 projected on (001), for a random tetrahedral cation configuration

d_2 distance between the tetrahedral cation and basal oxygen O2 projected on (001) for a random tetrahedral cation configuration

d_{13}^{I}, d_{13}^{II} distances at the tetrahedral sites I and II between the tetrahedral cations and the midpoints of the lines connecting the basal oxygens O1 and O3 projected on (001), for ordered tetrahedral cation configurations

d_2^{I}, d_2^{II} distances at the tetrahedral sites I and II between the tetrahedral cation and basal oxygen O2 projected on (001) in the case of ordered tetrahedral cation configurations

$d(100)$ d-spacing of (001) planes

$f_{o,i}$ mole fraction of the cation i in the octahedral site

$f_{t,j}$ mole fraction of cation j in the tetrahedral site, for a random tetrahedral cation configuration

$f_{t1,j}$, $f_{t2,j}$ mole fraction of cation j in the tetrahedral site I and II, respectively, for ordered tetrahedral cation configurations

h_h higher height of the tetrahedra along [001]

h_l lower height of the tetrahedra along [001]

l_o octahedral edge length for trioctahedral minerals

l_{os} shorter octahedral edge length for dioctahedral minerals

l_t tetrahedral edge length

n_k number of cation k in the chemical formula based on $O_{10}(OH)_2$

r_i average interatomic distance between the interlayer cation and the oxygen forming the inner triad

r_o average interatomic distance between the octahedral cation and oxygen

r_{o1}, r_{o2} average interatomic distance between the octahedral cations and oxygen at the octahedral site I and II

$r_{o,i}$ interatomic distance between the octahedral cation i and oxygen

r_t average interatomic distance between the tetrahedral cation and the oxygens, for a random tetrahedral cation configuration

r_{t1}, r_{t2} average interatomic distance between the tetrahedral cation and the oxygens in the tetrahedral site I and II, respectively, for ordered tetrahedral cation configurations

r_{tj} interatomic distance between the tetrahedral cation j and oxygen

r_t', r_{t1}', r_{t2}' interatomic distance between the tetrahedral cation and apical oxygen after the tetrahedral stretching

Y_c the shortest distance between the octahedral oxygens shared by the tetrahedra

Y_t shortest distance between the apical oxygens before tilting

x_k, y_k, z_k atomic coordinates of structural site k

α tetrahedral rotation angle

β interaxial angle between a- and c-axis in the second crystallographic

β setting

δ tetrahedral tilting angle before the stretching of the tetrahedra, for a random tetrahedral cation configuration

δ_1, δ_2 tetrahedral tilting angle of the site I and II before the tetrahedral stretching, respectively, for ordered tetrahedral configurations

η angle of the short octahedral edge to (001) before the increasing the vertical angle of octahedral edge

θ tetrahedral tilting angle after the tetrahedral stretching, for a random tetrahedral cation configuration

θ_1, θ_2 tetrahedral tilting angle of site I and II after tetrahedral stretching, for ordered tetrahedral cation configurations

θ', θ_1', θ_2' angles of the lines connecting the tetrahedral cation and the apical oxygen to (001) after the tetrahedral stretching

ξ_H amount of increase in the vertical angle of the octahedral OH-OH edge

ξ_O amount of increase in the vertical angle of the short octahedral O-O edge

χ rotation angle of the inner triad of the basal oxygen

Ψ angle between [001] and the line connecting the opposite vertices of the octahedron

ω flattening angle of the octahedron

All angles are in degrees and all distances, lengths, spacings, and heights are in Angstroms.

ACKNOWLEDGMENTS

Part of this study is financially supported by KOSEF grant #913-0501-001-2, given to the senior author. We thank Dr. S. Han for the discussion during the stage of the geometrical model development.

REFERENCES

Appelo, C. A. J. (1978) Layer deformation and crystal energy of micas and related minerals. I. Structural models for 1M and $2M_1$ polytypes. Am. Miner., 63, 782-792.

Bailey, S. W. (1984) Crystal chemistry of true micas. In: Bailey, S. W. (Ed.), Micas. Rev. Miner., 13, 13-60.

Collins, D. R. and Catlow, C. R. A. (1992) Computer simulation of structures and cohesive properties of micas. Am. Miner., 77, 1172-1181.

Donnay, G., Donnay, J. D. H., and Takeda, H. (1964) Trioctahedral one layer micas. II. Prediction of the structure from composition and cell dimensions. Acta Cryst., 17, 1374-1381.

Drits, V. A. and Zviagina, S. (1992) Relations between unit-cell parameters and cation composition of sheet silicates. I: White micas. Geologica Carpathica-Series Clays 1, 31-34, Bratislava.

Faust, G. T. (1957) The relation between lattice parameters and composition for montmorillonite-group minerals. J. Washington Acad. Sci., 47, 146-147.

Franzini, M. and Schiaffino, L. (1963) On the crystal structure of biotite. Zeit. Kristall., 19, 297-309.

Frey, M., Hunziker, Y. C., Jager, E., and Stern, W. (1983) Regional distribution of white K-mica polymorphs and their phengite content in the Central Alps. Contrib. to Miner. Petrol., 83, 185-197.

Guggenheim, S. and Bailey, S. W. (1975) Refinement of the margarite structure in subgroup symmetry. Am. Miner., 60, 1023-1029.

Guidotti, C. V. (1984) Micas in metamorphic rocks. In: Bailey, S. W. (Ed.), Micas. Rev. Miner., 13, 357-468.

G ven, N. (1971) The crystal structure of $2M_1$ phengite and $2M_1$ muscovite. Zeit. Kristall., 134, 196-212.

Hazen, R. M. and Burnham, C. W. (1973) The crystal structures of one-layer phlogopite and annite. Amer. Miner., 58, 889-900.

Radoslovich, E. W. (1962) The cell dimensions and symmetry of layer-lattice silicates. II. Regression relations. Amer. Miner., 47, 617-636.

Sadanaga, R. and Takeuchi, Y. (1961) Zeit. Kristall., 116, 406.

Shannon, R. D. (1976) Revised effective ionic radii and systematic studies of interatomic distances in halides and chalcogenides. Acta Cryst., 232, 751-767.

Sidorenko, O. V., Zvyagin, B. B., and Soboleva, S. V. (1975) Crystal structure refinement for 1M dioctahedral mica. Soviet Phys. Cryst., 20, 332-335.

Smoliar-Zviagina, B. B. (1993) Relationships between structural parameters and chemical composition of micas. Clay Miner., 28, 603-624.

Takeuchi, Y. (1965) Structures of brittle micas. Clays Clay Miner., 13, 1-25.

Tepkin, E. V., Drits, V. A., and Alexandrova, V. A. (1969) Crystal structure of iron biotite and construction of dtructural models for trioctahedral micas. Proceedings of International Clay Conference, Tokyo, 43-49.

Veitch, L. G. and Radoslovich, E. V. (1963) The cell dimensions and symmetry of layer-lattice silicates. III. Octahedral ordering. Amer. Miner., 48, 62-75.

Yu, J-Y. (1990) A Geometrical structural model of 2:1 trioctahedral clay minerals. J. Miner. Soc. Korea, 4, 90-98.